EarthArXiv Cover Sheet

Title:

Hydraulic geometry hypothesis allows reverse engineering of 3D quasi-equilibrium landscapes from 2D channel networks

Authors

Li Zhang[1] (ORCID: 0000-0002-9838-2718)
Dnyanesh Borse[2] (ORCID: 0000-0002-5140-2427)
Arvind Singh[2] (ORCID: 0000-0003-2172-6321)
James E. Pizzuto[3] (ORCID: 0000-0002-7978-7322)
Xudong Fu[4] ORCID: 0000-0003-0744-0546)
Gary Parker[5] (ORCID: 0000-0001-5973-5296)

[1]School of Water Resources and Hydropower Engineering, North China Electric Power University, Beijing 102206, China.
[2]Dept. of Civil, Environmental and Construction Engineering, University of Central Florida, Orlando 32816, USA.
[3]Dept. of Earth Sciences, University of Delaware, Newark 19716, USA.
[4]State Key Laboratory of Hydroscience and Engineering, Department of Hydraulic Engineering, Tsinghua University, Beijing 100084, China.
[5]Dept. of Earth Science & Environmental Change and Dept. of Civil & Environmental Engineering, University of Illinois Urbana-Champaign, Urbana 61801, USA.

Main Manuscript for

Hydraulic geometry hypothesis allows reverse engineering of 3D quasi-equilibrium landscapes from 2D channel networks

Li Zhang[1](ORCID: 0000-0002-9838-2718), Dnyanesh Borse[2](ORCID: 0000-0002-5140-2427), Arvind Singh[2](ORCID: 0000-0003-2172-6321), James E. Pizzuto[3] (ORCID: 0000-0002-7978-7322), Xudong Fu[4](ORCID: 0000-0003-0744-0546) and Gary Parker[5*](ORCID: 0000-0001-5973-5296)

[1]School of Water Resources and Hydropower Engineering, North China Electric Power University, Beijing 102206, China.

[2]Dept. of Civil, Environmental and Construction Engineering, University of Central Florida, Orlando 32816, USA.

[3]Dept. of Earth Sciences, University of Delaware, Newark 19716, USA.

[4]State Key Laboratory of Hydroscience and Engineering, Department of Hydraulic Engineering, Tsinghua University, Beijing 100084, China.

[5]Dept. of Earth Science & Environmental Change and Dept. of Civil & Environmental Engineering, University of Illinois Urbana-Champaign, Urbana 61801, USA.

*Gary Parker

Email: parkerg@illinois.edu

Author Contributions: Zhang: conceptualization and implementation of initial version of model; Borse: design and implementation of final version of model; Singh: guidance on drainage networks and landscape structure; Pizzuto: guidance on connection between hydraulic geometry and catchments; Fu: guidance on sediment transport within catchments; Parker: problem conceptualization and overall integration.

Competing Interest Statement: The authors declare no competing interests.

Classification: Major classification: Physical sciences. Minor classification: Earth, atmospheric and planetary sciences.

Keywords: drainage basins, fluvial landscape, network-generating algorithm, hydraulic geometry, reverse engineering

Abstract
A fluvial catchment consists of unchannelized hillslopes drained by a channel network. Catchments can be fully characterized by their three-dimensional (3D) topography and the bankfull characteristics of their channels. Here we use a probabilistic algorithm to generate a set of scale-free, two-dimensional (2D) pixelized river networks of increasing complexity. We then integrate reach-scale hydraulic geometry equations, originally developed for single-channel gravel-bedded river reaches, to reverse engineer the corresponding 3D landscape topography of these 2D synthetic networks (Reverse Engineered Fluvial Landscape, REFL). To do so requires specification of outlet flood discharge and a characteristic bed grain size. By incorporating hillslope-channel coupling, represented by a characteristic hillslope length and slope, we can fully specify the 3D topography of the entire watershed. Our results suggest that under appropriate constraints, the equilibrium hydraulic geometry hypothesis can be extended beyond isolated river reaches to encompass entire fluvial landscapes. The class of landscapes we consider are relatively low-slope montane catchments with subdued tectonics. The streams that drain the catchment are assumed to be alluvial or quasi-alluvial well upstream of the outlet. A simplified model analogous to the subgrid model of the Large Eddy Simulation model of turbulent flow is used to describe processes upstream of the limit of alluviated channels.

Significance Statement
Algorithmically generated pixel-based 2D river networks can be combined with relations for bankfull hydraulic geometry and simple assumptions characterizing hillslopes to reverse engineer realistic 3D fluvial landscapes with a full range of dimensionally correct attributes.

Introduction

Fluvial systems shape landscapes and provide the underpinnings that support aquatic habitat vital to humans and other life forms (1, 2, 3). Fluvial systems are organized into drainage basins. Drainage basins are further divided into hillslopes and channels, and are characterized by their shape, size and topography. Channels viewed in two-dimensions (2D) at the drainage basin scale appear dendritic, and create patterns similar to those of trees, leaf veins, blood circulatory systems, lightning patterns and agglomerates of charged metal particles (4, 5). River channel and ecological processes are also important at the scale of individual cross-sections, and are governed by a river's bankfull width, depth, slope and bed material grain size.

Many previous studies have sought to define and explain the physical structure of drainage basins. Landscape evolution models are powerful tools for predicting the topography of fluvial systems, including the geometry of fluvial networks (6, 7, 8, 9, 10, 11, 12). River channels, however, are not resolved by most landscape evolution models, and thus fluvial processes and morphology at these scales remain undefined. Channel networks are now routinely extracted from remotely-sensed three-dimensional (3D) topographic data such as Digital Elevation Models (DEM), providing an efficient methodology for defining fluvial networks from drainage basin topography (13, 14, 15, 16, 17, 18, 19). These methods, however, require rather than predict watershed topography, and they also fail to define fluvial morphology at the scale of the channel cross-section.

In this study we propose an approach to predict the physical structure of drainage basins that includes bankfull channel geometry, in addition to the channel network and the topography of the drainage basin. Instead of extracting 2D networks from 3D landscapes and assigning attributes in forward mode, we proceed in the opposite direction. We employ a scale-free, pixel-based probabilistic algorithm to generate 2D river networks. Then, physically-based and dimensionally homogeneous relationships for the bankfull geometry of channels within the river network are imposed to *reverse engineer* and scale up the associated 3D fluvial landscape. The 3D landscapes we assemble are fully scalable, representing elevation in meters, bankfull discharge in cubic meters per second, and so on. Such *reverse engineering* can be a valuable approach in geoscience, allowing researchers to infer the governing processes of an entire catchment. We refer to landscapes generated by this method as **Reverse Engineered Fluvial Landscapes** (**REFL**).

Our methods are extensions of the previous studies of Pizzuto (20, 21), Abed-Elmdoust et al. (22) and Balister et al. (23). Pizzuto (20, 21) combined physically-based hydraulic geometry equations and a steady-state sediment routing formulation to *reverse engineer* the 3D structure, bankfull channel geometry, and grain size of a stream network in central Pennsylvania, U.S.A. Pizzuto's results, however, do not include hillslopes, and thus they cannot reconstruct the topography of entire drainage basins. Abed-Elmdoust et al. (22), Balister et al. (23) and Carraro (24) created 3D drainage basins from the 2D optimal channel network (OCN) algorithm (25, 26, 3) by integrating a slope-area relationship. While their use of OCN has led to numerous advances, their work does not explicitly distinguish between hillslopes and channels, and lacks quantitative assessments of channel attributes such as bankfull discharge, width, depth and grain size.

Creating a scale-free, pixel-based 2D channel network is the first step in our analysis. Network generating algorithms for this purpose have a long history, dating back to at least the 1960's (27, 28). There have been substantial contributions and advancements since that time, including Howard (29, 30), Rinaldo et al. (25), Troutman and Karlinger (31), Rigon et al. (26), Sun et al. (32), Paik and Kumar (4, 33), Carraro et al. (24) and Borse and Biswal (34). The applicability of such 2D algorithmic representations to actual fluvial networks has been evaluated using metrics such as Hack's Law (35), Horton-Strahler stream ordering (36), scaling of contributing areas and upstream lengths (37, 38), the Gravelius compactness coefficient (39) and Tokunaga tree structure (40, 22, 41, 42).

The 2D network generating algorithm used in this analysis is that of Borse and Biswal (34). This model simulates headward growth using two parameters (downstream length and flow accumulation) to assign probabilities governing the direction of headward channel extension, resulting in networks that reproduce realistic tree-like river networks. The model can be applied within a given catchment divide. The networks so generated exhibit power-law scaling exponents in drainage area and link length, as well as basin shape characteristics consistent with a class of natural river catchments. Details of the algorithm are described in *Materials and Methods*. Other generation models of 2D networks such as the OCN model may also produce networks that are statistically similar to natural networks, but the model of Borse and Biswal (34) requires only two parameters to generate networks with varying shapes and topologies.

The next step in our analysis is the reverse engineering of a 2D generated network to a 3D drainage basin in which channels are explicitly included. We specify channel characteristics in terms of relations for bankfull hydraulic geometry. The downstream hydraulic geometry concept was first introduced by Leopold and Maddock (43), who determined how channel bankfull width (B_{bf}) and bankfull depth (H_{bf}) vary with increasing bankfull discharge (Q_{bf}) progressing downstream along a single channel. The concept has since been generalized to include channel slope (S) as an added dependent variable (44), and to consider not only multiple cross-sections along a single channel, but also multiple channels of different streams in different locations (45). It has recently been shown that several aspects of these relations (in particular coefficients and exponents) can be quantified using large sets of data (46, 47). Chang et al. (48) acquired such a set by means of remote sensing and analyzed it using machine learning. These capabilities invite inquiry as to the physical basis underlying these relations (49).

The bankfull hydraulic geometry relationships used in this analysis were developed for self-formed, quasi-equilibrium, alluvial, gravel-bedded rivers (50). These relationships have a full physical basis, including quantification of momentum and mass balance, channel resistance, channel-forming Shields number, and a sediment transport relation. They are dimensionally homogeneous and therefore freely scalable.

The target watersheds we consider are mountain catchments with gravel-bed streams that actively transport their gravel, but which have relatively low relief and subdued tectonics. We use the database of 62 British gravel-bed streams in Hey and Thorne (51) in order to develop and test our procedure for reverse engineering. Further caveats to the analysis are outlined below.

Pixel-based Synthetic 2D Fluvial Networks of Increasing Complexity

We generated four scale-free channel networks (Fig. 1 *A*-*D*) with a single outlet and a grid-size of ~350×300 using the network generating algorithm described in *Materials and Methods*. These synthetic 2D river networks are named as follows: RN_{2D}-1, RN_{2D}-2, RN_{2D}-3, RN_{2D}-4 in sequence (as shown in Fig. 1 *A*-*D*). All networks are embedded within a common catchment divide. The number and lengths of channels in these networks increase progressively from RN_{2D}-1 (Fig. 1*A*) through RN_{2D}-4 (Fig. 1*D*), which we characterize as increasing network complexity. RN_{2D}-3, RN_{2D}-2 and RN_{2D}-1 can also be described as the successive pruning of RN_{2D}-4. Strahler orders for these four networks are 3 (RN_{2D}-1), 4 (RN_{2D}-2 and 3) and 5 (RN_{2D}-4) (Table 1). We have also included information about an extra fifth network in Table 1, i.e. RN_{2D}-5, which is a step more complex than RN_{2D}-4, and used for testing model behavior at large scale.

Dimensionless Hydraulic Geometry for Gravel-Bed Streams

Parker et al. (50) developed dimensionless relations for bankfull hydraulic geometry of alluvial gravel-bed rivers using a) a database consisting of 16 reaches from Alberta Canada, 23 reaches from the Britain, 23 reaches from Idaho USA, and 10 reaches from Colorado USA, and b) a set of relations encompassing mass balance, momentum balance, channel resistance, a bedload transport equation applicable to gravel and a relation for channel-forming Shields number. These relations take the following form:

$$\tilde{B} = 4.63\hat{Q}^{0.0667} \qquad [1a]$$

$$\tilde{H} = 0.382\hat{Q}^{0.0004} \qquad [1b]$$

$$S = 0.101\hat{Q}^{-0.344} \qquad [1c]$$

where

$$\hat{Q} = \frac{Q_{bf}}{\sqrt{gD}D^2}, \quad \tilde{B} = \frac{g^{1/5}B_{bf}}{Q_{bf}^{2/5}}, \quad \tilde{H} = \frac{g^{1/5}H_{bf}}{Q_{bf}^{2/5}} \qquad [1d]$$

and Q_{bf} = bankfull channel discharge, H_{bf} = bankfull depth, B_{bf} = bankfull width, S = streamwise channel slope, D = characteristic bed material size, g = gravitational acceleration, $\tilde{B}$ = dimensionless channel width, $\tilde{H}$ = dimensionless channel depth, $\hat{Q}$ = dimensionless flow discharge. These relations implicitly assume a sediment specific gravity of 2.65, i.e. the standard value for quartz.

We use these relations as follows. If bankfull discharge Q_{bf} is known at any channel cross-section in the network, then bankfull width B_{bf}, bankfull depth H_{bf} and channel slope S can be computed from Eqs. **1a-d**.

Empirical Relation between Bankfull discharge and Catchment Area from Field Data

The above hydraulic geometry relations, i.e. Eqs. **1a-d**, were tested against a second set of 62 reaches of British alluvial gravel-bed streams from Hey and Thorne (51), here referred to as Britain II, and found to perform well. The Britain II data set, which is given as Table S1 in the *SI Appendix*, is particularly valuable because in addition to including bankfull parameters and characteristic grain sizes, it also includes the drainage area upstream of the relevant cross-section. This makes this data set ideal for the *reverse engineering* of the 2D pixelized Networks RN_{2D}-1 to RN_{2D}-4.

We use the following empirical relation for discharge Q_{bf} as a function of catchment area A for the Britain II streams (51) based on the regression shown in Fig. 1*F*:

$$Q_{bf} = 3.11A^{0.61} \qquad [2]$$

The above equation is not dimensionally homogeneous and cannot be assumed to be universal. For example, it does not include the effect of variation in precipitation rate or type from catchment to catchment, or within a catchment. In addition, it is applicable specifically to the Britain II catchments. We use Eq. **2** here as an example of the relationship between discharge and area. It can be replaced by any other relation found to be applicable to some other set of gravel-bed streams, or which includes dependency on other parameters.

The use of the above relations in the context of the Britain II catchments places several restrictions on the upscaling: a) the streams in the network are alluvial; b) the bed is everywhere characterized by a single grain size D, so that downstream fining is not considered; and c) the setting is that of a montane catchment of relatively low relief and subdued tectonics. It is likely, however, that sufficiently far upstream in the catchment, the streams in the network are mixed bedrock-alluvial rather than purely alluvial (52, 53, 54). In addition, non-fluvial processes such as in-channel landslides may become important toward the headwaters of each channel (55, 56, 57). We deal with these issues by assuming a constant “effective hillslope length” L_h that is longer than the range characteristically found for mountain catchments (58), and a constant “effective hillslope slope” S_h that is calibrated to the five Britain II catchments described in Fig. S1 the *SI Appendix*. This formulation bears analogy to the characterization of subgrid scales used in the Large Eddy Simulation model of turbulent flow (58).

Having outlined the above restrictions and caveats, we emphasize that we are not reproducing the structure of any specific mountain catchment, either within the Britain II set or without it. The details of channel structure in each catchment can be expected to depend on local variations in rock type, soil erodibility, precipitation patterns, and also purely random factors. Rather, our goal is to *reverse engineer* 3D catchments that are statistically equivalent to those in the Britain II set, and are potentially generalizable to other low-relief, tectonically subdued montane landscapes.

Reverse Engineering of 2D Pixel-based Networks to 3D Landscapes with Dimensions

We can assign a scale to the 2D channel networks by assigning a dimensioned size (m^2) to each pixel. To do so we specified dimensioned values of drainage density (D_d) and hillslope length (L_h) for our field landscapes. For any given drainage network, drainage density D_d can be defined as

$$D_d = \frac{\sum L}{A_T} \qquad [3]$$

where A_T is the total area of the catchment and ΣL is the corresponding total length of channels (60). Furthermore, a characteristic hillslope length L_h can be defined as

$$L_h = \frac{1}{2D_d} \qquad [4]$$

The raster on which the drainage networks of Networks 1-4 are generated is the same 350 x 300 pixels in all cases. The catchment divide is also precisely the same in all cases. As the network length increases from RN_{2D}-1 to RN_{2D}-4, the corresponding drainage density in pixel units D_{dp} increases from 0.03 to 0.14 (Table 1). We scale up from hillslope length L_{hp} in pixels to field hillslope length L_h in meters using the relation

$$L_h = \lambda L_{hp} = \frac{\lambda}{2D_{dp}} \qquad [5]$$

where λ is a scale factor between field and pixel hillslope lengths. We assume that the field hillslope length L_h takes the same value for all four catchments corresponding to Networks 1-4, so λ increases with increasing network complexity.

Grieve et al. (58) report that hillslope lengths L_h vary from 33 m to 58 m, or ~ 50 m for four montane topographic regions based on drainage density. Meghani and Anders (61) report asymptotic post-glaciation hillslope lengths of about 360 m in the upper Midwest lowlands of the United States based on partial drainage density. Hillslope lengths for the Britain II streams are likely between these two ranges, but closer to the former. In preliminary upscaling calculations for the Britain II streams, however, it was found that hillslope length of 50 m corresponds to an unrealistic extension of our relations for hydraulic geometry of alluvial streams. As discussed above, this is likely because a) downstream fining of bed material is not characterized in the analysis, and b) the streams are probably not purely alluvial all the way to their headwaters. To address this issue, we extracted DEMs for five of the catchments of the Britain II set and determined an "effective hillslope length" L_h of 500 m from them. The same analysis gave an "effective hillslope slope" S_h of 0.10 Details of the analysis are presented in the *SI Appendix*.

RN_{2D}-1-4 of Fig. 1*A*-1*D* are scaled up with the scale factors λ of 33.3, 49.3, 76.7 and 103.6 in Table 1. Correspondingly, their total area and total length are (A_T, ΣL) = (69.23 km^2, 69.23 km), (152.36 km^2, 152,36 km), (367.78 km^2, 367.78 km) and (671.26 km, 671.26 km^2). In all five cases in Table 1 this yields a field-scale drainage density D_d of 0.001 m^{-1} and a corresponding hillslope length L_h of 500 m. This range of areas was chosen to fall within the range of the Britain II stream sizes for which drainage area are reported (59 of 62 sites): 9.1 km^2 to 1500 km^2 (with a mean of 206 km^2).

The implementation of Eqs. **1a-d** to compute bankfull channel parameters requires a characteristic bed material grain size D. Here we use the value D = 59 mm based on the average value for the Britain II sites for which bed grain size is reported. (The range is 14 mm to 176 m).

The catchment area *A* at every channel node in the synthetic catchments RN_{2D}-1 to RN_{2D}-4 is scaled up according to the factor λ^2. The bankfull discharge Q_{bf} at each channel node is then calculated from Eq. **2**. Bankfull width B_{bf}, bankfull depth H_{bf} and channel slope S are then computed at every channel node from Eqs. **1a-d** from Q_{bf} is and grain size D. Maximum and minimum values of B_{bf}, H_{bf} and S of each *reverse engineered* 3D drainage basin are listed in Table 1.

Once channel slope S is known at every channel point, a numerical integration allows the computation of elevation above the catchment mouth at every channel node η. The elevations of hillslope nodes η_h are then computed using hillslope slope S_h = 0.10 and the distance from each hillslope node to the nearest channel.

Results of Reverse Engineering: Field-scale Synthetic Landscapes

Figs. 2*A-D* show the *reverse engineered* fluvial landscapes (abbreviated here as REFL) for RN_{2D}-1 - RN_{2D}-4, upscaled according to the above procedures. Fig. 2*E* shows the long profiles of the main-stem channels. For reference, Fig. S1 of the *SI Appendix* shows fluvial landscapes extracted from DEMs based on remote sensing for five catchments selected from the Britain II set. It is not expected that any of our synthetic landscapes should reproduce the details of any of the British landscapes. Of more relevance are the hypsometric curves (indicating the proportion of land area that lies at or above a specified elevation) of Fig. 2*F*, which include four curves of RL_{3D}-1 - RL_{3D}-4 (corresponding to Figs. 2*A* - 2*D*) and a mean curve for the five Britain II catchments of Fig. S1 *A-E*. It is seen that our methodology provides reasonable agreement with the mean hypsometric curve based on field data. In addition, the average relief of the REFLs is around 500 m, a value that compares well with all but one of the Britain II catchments in Table S2 of the *SI Appendix*.

Figs. 3*A* and 3*B* provide 3D views of the REFL corresponding to RN_{2D}-1 and RN_{2D}-4 of Figs. 2*A* and 2*D*. Fig. 3C shows the form of Hack's Law obeyed by our synthetic basins. The coefficient is 1.64 and the exponent is 0.55. The Gravelius compaction coefficient for all our catchments, including RL_{3D}-1 – RL_{3D}-5, is 1.55. These three values are consistent with the most common field-scale catchments in Sassolas-Serrayet et al. (39); see Fig. 5 therein. Fig. 3*D* shows the power-law scaling of areas for the four REFLs RL_{3D}-1 – RL_{3D}4. Here the area scaling exponent is seen to be β = 0.43, a value that is close to field rivers (i.e. 0.43 ± 0.03 in reference 4, Table 1 therein; 0.46 in reference 62, Fig.5 therein). Our REFLs are thus in good compliance with scaling laws for field fluvial landscapes.

Fig. 4 shows the set of channel attributes obtained from the RL_{3D}-1 and RL_{3D}-4. Figs. 4*A* and 4*E* show corresponding elevation profiles for the main stem and all tributaries in the catchments. Such elevation profiles are routinely generated from DEMs of remotely-sensed field data; an example is shown in Fig. S6 of the *SI Appendix* (63). Figs. 4*A* and 4*E* show that these profiles can also be generated by reverse engineering.

Figs. 4*B* - 4*D* show bankfull discharge Q_{bf}, bankfull width B_{bf} and bankfull depth H_{bf}, respectively, at every point of every channel of the scaled-up landscape RL_{3D}-1 generated from RN_{2D}-1. Figs. 4*E*-*G* show the corresponding plots for RL_{3D}-4 generated from RN_{2D}-4. All plots are organized according to main stem and tributaries in analogy to Figs. 4*A* and 4*E*. Bankfull discharge and bankfull depth in particular are not generally accessible via remote sensing. Our *reverse engineering* technique, however, allows us to describe these parameters throughout the catchments via physically-based relations that are well-grounded in field data. The level of detail with which attributes are characterized by the REFL methodology may provide useful information for ecosystem analysis within a catchment.

The above analysis demonstrates the feasibility of generating realistic REFL representations of fluvial landscapes based on two components. The first of these consists of pixel-based 2D networks that are known to satisfy characteristics of fluvial networks. The second consists of relations for hydraulic geometry that are known to apply to alluvial gravel-bed rivers. When field-based empirical assumptions are added for hillslope length and hillslope slope, a complete description of low-relief montane catchment attributes can be obtained.

Our analysis does have limitations, in that a) a relation for bankfull discharge versus catchment area and values for "effective hillslope length" and "effective hillslope slope" were obtained on a site-specific basis for the Britain II set of field data, and b) the effects of downstream fining and the presence of mixed bedrock-alluvial channels in the upper parts of the catchments are not captured (See Fig S5 of the *SI Appendix*). Many of the components needed to complete these parts of the puzzle are, however, already available (64, 65, 52, 53, 54). This suggests a promising path forward for future research into the reverse engineering of fluvial landscapes.

Materials and Methods

We generate our 2D networks using the scale-free network generation algorithm of Borse and Biswal (34). This model can be applied to a catchment with an arbitrarily-shaped boundary (divide) upon the specification of the location of outlets. In particular, we apply this algorithm within a randomly generated sample basin boundary with a single specified outlet. The algorithm simulates headward growth of channel networks starting from the outlet by adding one adjacent pixel per step to the growing network. In this manner, the algorithm assigns flow directions to all the pixels in the catchment.

The network generating algorithm of Borse and Biswal (34) proceeds as follows. 1) The selection of a potential pixel for network growth is based on the proportionality to the downstream length l of a network evolved in the previous step, expressed as $P_{\text{select}} \propto l^{\alpha}$. Thus, for any positive value of α, the channel with a longer downstream distance will have a higher probability to grow headward. 2) Once a pixel is selected, its flow direction is chosen by evaluating the flow accumulation (A_d) of its adjacent evolved pixels. The model assigns flow directions (and thus flow accumulation areas) based on the eight pixels adjacent to any given pixel. Flow direction is decided probabilistically using $P_{\text{flow}} \propto A_d{}^{\beta}$. Thus, for positive values of β, there is a higher preference for choosing the flow direction toward pixels with greater flow accumulation area. This model offers flexibility in generating networks of varying characteristics by controlling the choices of α and β. At the same time, the method preserves the statistical scaling properties of field river networks. See Borse and Biswal (34) for more details. Here we used $\alpha = 1$ and $\beta = 1$ for generating networks within the basin boundary corresponding to a grid-size ~ 350×300, with the single outlet shown in Figs. 1*A*-1*D*. We then apply different flow accumulation thresholds to extract channel networks of varying drainage density.

Using the upscaled, dimensioned area A obtained from the flow accumulation area draining into each pixel, we compute the dimensioned bankfull discharge Q_{bf} there via Eq. **2**. We use Eq. **1a-b and d** to calculate the bankfull width B_{bf} and depth H_{bf} for each channel point as shown in Figs. 4 *C*, *D*, *G* and *H*. Eq. **1c** also provides slope values S for each channel pixel. Assuming the outlet elevation to be zero, we traverse upward along the flow paths and assign an elevation η to every channel pixel upstream according to the following rule for numerical integration: $\eta_{i+1} = \eta_i + \Delta x\, S$. Here η_i represents the elevation of a channel pixel i, and η_{i+1} is the elevation of channel pixel $i + 1$ immediately upstream of pixel i. The value of Δx is either the upscaled pixel size or $\sqrt{2}$ times the upscaled pixel size, depending on whether the flow direction is cardinal or diagonal. As noted above, the slope for hillslope pixels S_h is assumed to be constant at 0.10. This slope is used to calculate hillslope elevation η_h at any upscaled pixel.

Acknowledgments

Gordon Grant suggested the term "reverse engineering". Joel Scheingross and Scott McCoy provided valuable advice.

References

1. F. Carrara, F. Altermatt, I. Rodríguez-Iturbe, A. Rinaldo, Dendritic connectivity controls biodiversity patterns in experimental metacommunities. *Proc. Natl. Acad. Sci. U.S.A.* **109**, 5761-5766 (2012).
2. I. Rodríguez-Iturbe, R. Muneepeerakul, E. Bertuzzo, S. A. Levin, A. Rinaldo, River networks as ecological corridors: A complex systems perspective for integrating hydrologic, geomorphologic, and ecologic dynamics. *Water Resour. Res.* **45**, W01413 (2009).
3. I. Rodríguez-Iturbe, A. Rinaldo, Fractal river basins: chance and self-organization. *Cambridge University Press*, (1997).
4. K. Paik, P. Kumar, Emergence of self-similar tree network organization. *Complexity* **13**, 30-37 (2008).
5. J. D. Pelletier, D. L. Turcotte, Shapes of river networks and leaves: are they statistically similar?. *Phil. Trans. R. Soc. Lond. B.* **355**, 307-311 (2000).
6. G. Willgoose, R. L. Bras, I. Rodríguez-Iturbe, A physically based coupled network growth and hillslope evolution model: 1. Theory. *Water Resour. Res.* **27**, 1671-1684 (1991).

7. A. D. Howard, A detachment-limited model of drainage basin evolution. *Water Resour. Res.* **30**, 2261-2285 (1994).
8. G. E. Tucker, R. L. Bras, Hillslope processes, drainage density, and landscape morphology. *Water Resour. Res.* **34**, 2751-2764 (1998).
9. G. E. Tucker, G. R. Hancock, Modelling landscape evolution. *Earth Surf. Process. Landf*. **35**, 28-50 (2010).
10. A. Chen, J. Darbon, J. M. Morel, Landscape evolution models: A review of their fundamental equations. *Geomorphology* **219**, 68-86 (2014).
11. J. S. Kwang, A. L. Langsdon, G. Parker, The role of lateral erosion in the evolution of nondendritic drainage networks to dendricity and the persistence of dynamic networks. *Proc. Natl. Acad. Sci. U.S.A.* 118, e2015770118 (2021).
12. A. H. Bavojdan, S. Ranjbar, D. B. Wang, A. Singh, Signatures of varying climate on geomorphic and topologic characteristics of channel networks. Water Resour. Res. **61**, e2024WR038760 (2025).
13. J. F. O'Callaghan, D. M. Mark, The extraction of drainage networks from digital elevation data. *Computer Vision, Graphics, and Image Processing* **28**, 323-344 (1984).
14. D. R. Maidment, Arc Hydro GIS for Water Resources. *ESRI Press*, (2002).
15. M. Metz, H. Mitasova, R. S. Harmon, Efficient extraction of drainage networks from massive, radar-based elevation models with least cost path search. *Hydrol. Earth Syst. Sci.* **15**, 667-678 (2011).
16. M. Hooshyar, S. Kim, D. Wang, S. C. Medeiros. Wet channel network extraction by integrating LiDAR intensity and elevation data. *Water Resour. Res.* **51**, 10029-10046 (2015).
17. T. Wu, J. Y. Li, T. J. Li, B. Sivakumar, G. Zhang, G. Q. Wang, High-efficient extraction of drainage networks from digital elevation models constrained by enhanced flow enforcement from known river maps. *Geomorphology* **340**, 184-201 (2019).
18. D. Li, B. S. Wu, B. W. Chen, C. Qin, Y. J. Wang, Y. J. Zhang, Y. Xue, Open-surface river extraction based on Sentinel-2 MSI imagery and DEM data: case study of the upper Yellow River. *Remote Sens.* **12**, 2737 (2020).
19. P. Passalacqua, T. Do Trung, E. Foufoula-Georgiou, G. Sapiro, W. E. Dietrich, A geometric framework for channel network extraction from lidar: Nonlinear diffusion and geodesic paths. *J. Geophys. Res.* **115**, F01002 (2010).
20. J. E. Pizzuto, The morphology of graded gravel rivers: a network perspective. *Geomorphology* **5**, 457-474 (1992).
21. J. E. Pizzuto, Downstream fining in a network of gravel-bedded rivers. *Water Resour. Res.* **31**, 753-759 (1995).
22. A. Abed-Elmdoust, M. Mohammad-Ali, A. Singh, Reorganization of river networks under changing spatiotemporal precipitation patterns: An optimal channel network approach. *Water Resour. Res.* **52**, 8845-8860 (2016).
23. P. Balister, J. Balogh, E. Bertuzzo, B. Bollobás, G. Caldarelli, A. Maritan, R. Mastrandrea, R. Morris, A. Rinaldo, River landscapes and optimal channel networks. *roc. Natl. Acad. Sci. U.S.A.* **115**, 6548-6553 (2018).
24. L. Carraro, E. Bertuzzo, E. A. Fronhofer, R. Furrer, I. Gounand, A. Rinaldo, F. Altermatt, Generation and application of river network analogues for use in ecology and evolution. *Ecol Evol.* **10**, 7537-7550 (2020).
25. A. Rinaldo, I. Rodríguez-Iturbe, R. Rigon, R. L. Bras, E. Ijjasz-Vasquez, A. Marani, Minimum energy and fractal structures of drainage networks. *Water Resour. Res.* **28**, 2183-2195 (1992).
26. R. Rigon, A. Rinaldo, I. Rodríguez-Iturbe, R. L. Bras, E. Ijjasz-Vasquez, Optimal Channel Networks: a framework for the study of river basin morphology. *Water Resour. Res.* **29**, 1635-1646 (1993).
27. L. B. Leopold, W. B. Langbein, The concept of entropy in landscape evolution. *U.S. Geological Survey Professional Paper* **500-A**, A1-A20 (1962).
28. H. Schenck Jr., Simulation of the evolution of drainage-basin networks with a digital computer. *J. Geophys, Res.* **68**, 5739-5745 (1963).

29. A. D. Howard, Simulation of stream networks by headword growth and branching. *Geographical Analysis* **3**, 29-50 (1971).
30. A. D. Howard, Theoretical models of optimal drainage networks. *Water Resour. Res*. **26**, 2107-2117 (1990).
31. B. M. Troutman, M. R. Karlinger, Gibbs' Distribution on drainage networks. *Water Resour. Res.* **28**, 563-577 (1992).
32. T. Sun, P. Meakin, T. Jøssang, Minimum energy dissipation model for river basin geometry. *Phys. Rev. E* **49**, 4865-4872 (1994).
33. K. Paik, P. Kumar, Optimality approaches to describe characteristic fluvial patterns on landscapes. *Phil. Trans. R. Soc. B* **365**, 1387-1395 (2010).
34. D. Borse, B. Biswal, A novel probabilistic model to explain drainage network evolution. *Adv. Water Resour.* **171**, 104342 (2023).
35. J. T. Hack, Studies of longitudinal stream profiles in Virginia and Maryland. *U.S. Geological Survey Professional Paper* **294-B**, 45-95 (1957).
36. R. L. Shreve, Statistical law of stream numbers. *J. Geol.* **74**, 17-37 (1966).
37. A. Maritan, A. Rinaldo, R. Rigon, A. Giacometti, I. Rodríguez-Iturbe, Scaling laws for river networks. *Phys. Rev.* E **53**, 1510-1515 (1996).
38. P. S. Dodds, D. H. Rothman, Scaling, Universality, and Geomorphology. *Annu. Rev. Earth Planet. Sci*. **28**, 571-610 (2000).
39. T. Sassolas-Serrayet, R. Cattin, M. Ferry, The shape of watersheds. *Nat Commun* **9**, 3791 (2018).
40. S. D. Peckham, New results for self-similar trees with applications to river networks. *Water Resour. Res.* **31**, 1023-1029 (1995).
41. K. Y. Wang *et al*., Side tributary distribution of quasi-uniform iterative binary tree networks for river networks. *Front. Environ. Sci.* **9**, 792289 (2022).
42. Y. Kovchegov, I. Zaliapin, E. Foufoula-Georgiou, Random self-similar trees: emergence of scaling laws. *Surv Geophys* **43**, 353-421 (2022).
43. L. B. Leopold, T. Maddock, The hydraulic geometry of stream channels and some physiographic implications. *U.S. Geological Survey Professional Paper* **252**, 1-57 (1953).
44. R. D. Hey, Determinate hydraulic geometry of river channels. *Journal of the Hydraulics Division* **104**, 869-885 (1978).
45. G. Parker, Hydraulic geometry of active gravel rivers. *Journal of the Hydraulics Division* **105**, 1185-1201 (1979).
46. D. Li et al., A bankfull geometry dataset for major exorheic rivers on the Qinghai-Tibet Plateau. *Sci Data* **9**, 498 (2022).
47. T. Enzminger, J. Toby Minear, B. Livneh, HyG: A hydraulic geometry dataset derived from historical stream gage measurements across the conterminous US. *Sci Data* **11**, 1153 (2024).
48. S. Y. Chang et al., The geometry of flow: advancing predictions of river geometry with multi-model machine learning. *Water Resour. Res.* **60**, (2024).
49. C. B. Phillips et al., Thresholdk constraints on the size, shape and stability of alluvial rivers. *Nat Rev Earth Environ* **3**, 406-419 (2022).
50. G. Parker, P. Wilcock, C. Paola, W. Dietrich, Physical basis for quasi- universal relationships for bankfull hydraulic geometry of single-t hread gravel- bed rivers. *J. Geophys. Res.* **112**, F04005 (2007).
51. R. D. Hey, C. Thorne, Stable channels with mobile gravel beds. *J. Hydraul. Eng.* **112**, 671-689 (1986).
52. L. Zhang, T. J. Li, G. Q. Wang, J. S. Kwang, J. A. Nittrouer, X. D. Fu, G. Parker, How canyons evolve by incision into bedrock: Rainbow Canyon, Death Valley National Park, United States. *Proc. Natl. Acad. Sci. U.S.A*. **117**, 14730-14737 (2020).
53. L. Zhang, G. Parker, Source-to-sink canyon-fan Interaction in a closed basin. *Abstracts*, *European Geophysical Union General Assembly* Abstract, (2023).
54. M. O. Guirro, R. Hodge, F. Clubb, L. Turnbull, Network-scale dynamics of alluvial cover in a mixed bedrock-alluvial river. *J. Geophys. Res. Earth Surf.* **130**, e2024JF007968 (2025).

55. D. Montgomery, W. Dietrich, Where do channels begin?. *Nature* **336**, 232-234 (1988).
56. J. J. Roering, J. T. Perron, J. W. Kirchner, Functional relationships between denudation and hillslope form and relief. *Earth Planet. Sci. Lett.* **264**, 245-258 (2007).
57. S. W. McCoy et al., Sediment entrainment by debris flows: In situ measurements from the headwaters of a steep catchment. *J. Geophys. Res. Earth Surf.* **117**, F03016 (2012).
58. P. Sagaut, *Large Eddy Simulation for Incompressible Flows: an Introduction*. Springer Science & Business Media (2005).
59. S. W. D. Grieve, S. M. Mudd, M. D. Hurst, How long is a hillslope?. *Earth Surf. Process. Landforms* **41**, 1039-1054 (2016).
60. R. E. Horton, Drainage-basin characteristics. *Eos Trans. AGU* **13**, 350-361 (1932).
61. N. Meghani, A. Anders, Timescales of drainage network evolution revealed: spatiotemporal variability in drainage density in the post-glacial central lowlands, USA. *Am. J. Sci*. **325**, Article 2 (2025).
62. L. Cararro, F. Altermatt, Optimal Channel Networks accurately model ecologically-relevant geomorphological features of branching river networks. *Commun Earth Environ* **3**, 125 (2022).
63. J. A. Czuba et al., Geomorphic analysis of the river response to sedimentation downstream of Mount Rainier, Washington. *U.S. Geological Survey Open-File Report* **2012-1242**, 134p (2012).
64. P. Chatanantavet, E. Lajeunesse, G. Parker, L. Malverti, P. Meunier, Physically based model of downstream fining in bedrock streams with lateral input. *Water Resour. Res.* **46**, W02518 (2010).
65. R. I. Ferguson, B. P. Sharma, R. J. Hardy, R. A. Hodge, J. Warburton. Flow resistance and hydraulic geometry in contrasting reaches of a bedrock channel. *Water Resour. Res.* **53**, 2278-2293 (2017).

Figures and Tables

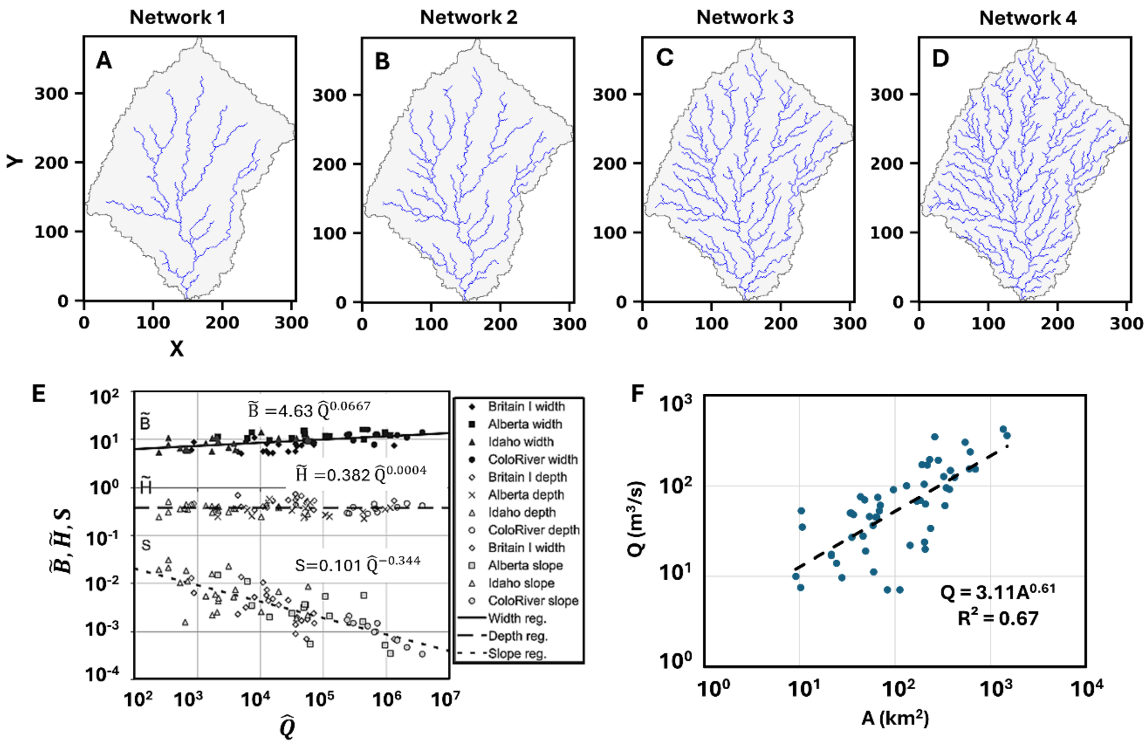

Fig. 1. Synthetic river networks and relations for hydraulic geometry and bankfull discharge. (*A-D*) Networks shown in A (RN_{2D}-1), B (RN_{2D}-2), C (RN_{2D}-3) and D (RN_{2D}-4) are obtained from the probabilistic 2D network generation algorithm of Borse and Biswal (34). Networks with increasing complexity. Networks 1 (RN_{2D}-1) to 4 (RN_{2D}-4) are obtained by pruning the network using flow accumulation thresholds of 1000, 500, 200 and 100 pixels, respectively. (*E*) The hydraulic geometry relationships for gravel bedded rivers (modified from reference 50 (Parker et al., 2007), Figure 1 therein). (*F*) The relationship between bankfull discharge Q_{bf} and drainage area A from the data of 62 British rivers given in Table S1 of the *SI Appendix*.

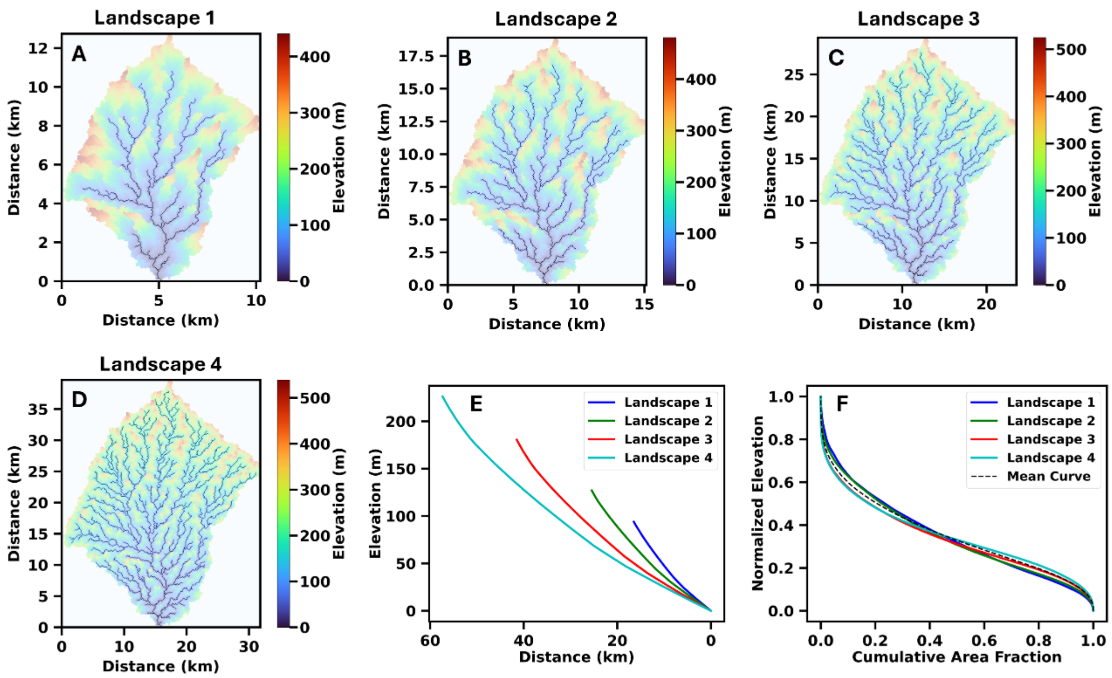

Fig. 2. Simulated drainage basin landscapes, river long profiles, and hypsometric curves. (*A-D*) A, B, C and D show the 3D REFL catchment landscapes RN_{3D}-1, RN_{3D}-2, RN_{3D}-3 and RN_{3D}-4, respectively. (*E*) The elevation profiles for the longest channels (main stems) in each of the four catchments. (*F*) The hypsometric curves for the four catchments. Also shown in (*F*) is a mean hypsometric curve for the 5 British catchments of the *SI Appendix*. More information is provided in Fig. 3.

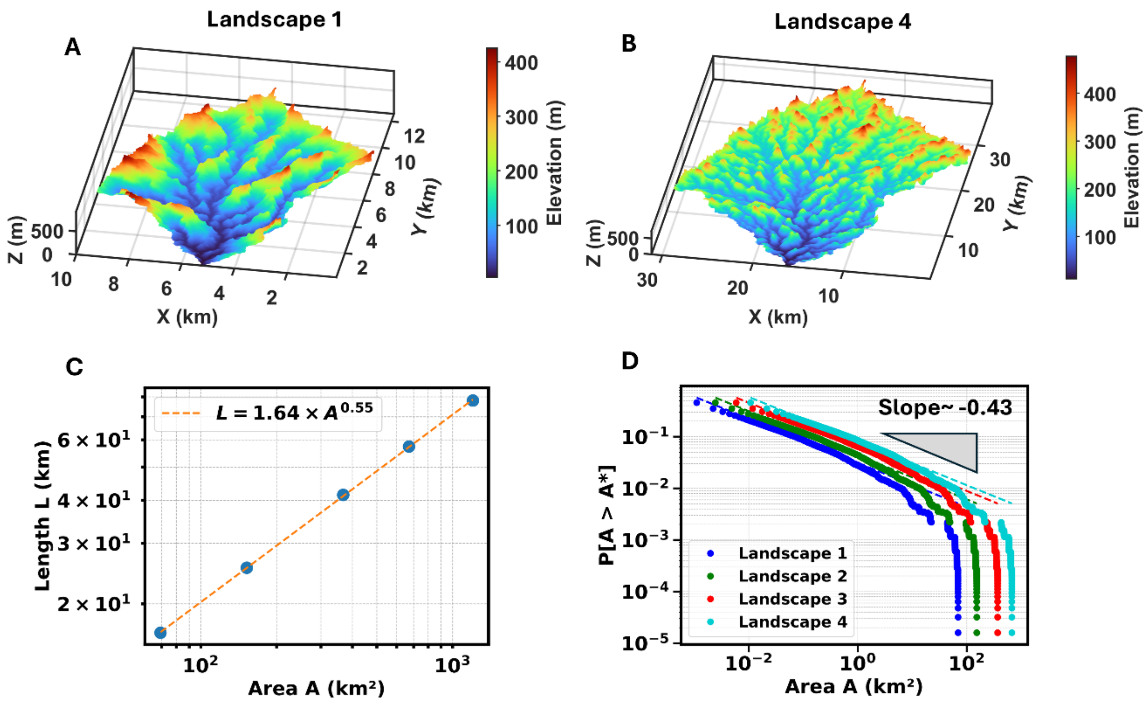

Fig. 3. Three-dimensional visualization of simulated landscapes and their geometric properties. (*A-B*) 3D REFL landscapes RN_{3D}-1 and RN_{3D}-4, obtained from 2D Networks 1 (RN_{2D}-1) and 4 ((RN_{2D}-4), respectively. (*C*) Hack's relationship obtained using the total area A and main channel length L of the four synthetic landscapes of Fig. 2 *A-D*, as well as Network 5 of Table 1 (the largest catchment considered here). (*D*) Modeled networks follow the scaling of drainage areas with a scaling exponent ~ 0.43 as observed in field river networks.

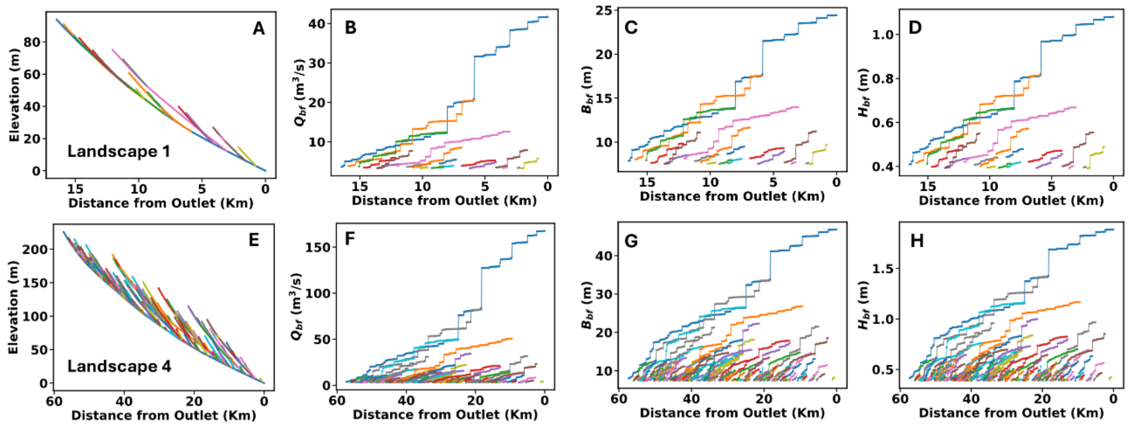

Fig. 4. Details of channel attributes along the channel reach for the REFL landscapes. (*A-D*) A, B, C and D shows elevation profile η, bankfull discharge Q_{bf}, bankfull width B_{bf} and bankfull depth H_{bf} , respectively, along the channels for first (smallest) catchment RN_{3D}-1 based on Network 1. (*E-H*) E, F, G and H show the corresponding attributes for the fourth catchment RN_{3D}-4 based on Network 4. The longest line in each plot corresponds the main stem. The plots illustrate the wealth of detailed information concerning channel attributes in a network that can be obtained from the REFL methodology.

Table 1 Details of the 2D simulated networks and corresponding REFL landscapes. Here D_{dp} represents pixelized drainage density.

Network	Stream order (Ω)	D_{dp}	Scale factor λ	Drain. area A_T (km^2)	ΣL (Km)	Q_{bf} (m^3/s)	Max. channel length (km)	Max. elev. (m)	Slope (outlet)	Min. bankfull width (m)	Max. bankfull width (m)	Min. bankfull depth (m)	Max. bankfull depth (m)
1	3	0.0333	33.3	69	69	42	16	441	0.0040	7.89	24.44	0.41	1.08
2	4	0.0493	49.3	152	152	68	25	481	0.0034	7.72	30.62	0.40	1.31
3	4	0.0767	76.7	368	368	116	41	525	0.0028	7.95	39.39	0.41	1.63
4	5	0.1036	103.6	671	671	168	57	539	0.0025	8.01	46.78	0.41	1.89
5	5	0.1387	138.7	1204	1204	240	78	532	0.0022	7.62	55.27	0.40	2.18

Supporting Information for

Hydraulic geometry hypothesis allows reverse-engineering of 3D quasi-equilibrium landscapes from 2D channel networks

Li Zhang, Dnyanesh Borse, Arvind Singh, James E. Pizzuto, Xudong Fu and Gary Parker*

*Corresponding author: Gary Parker

Email: parkerg@illinois.edi

This PDF file includes:

Supporting text

Figures S1 to S6

Tables S1 to S2

SI Reference

Supporting text

We obtained data on bankfull geometry at and drainage area above for 62 British channel sites from S. Darby, University of Nottingham, UK. The data correspond to that used in the analysis by Hey and Thorne (1986; see main text). We reproduce this data in Table S1. We selected the 5 basins of different drainage areas shown in that figure so as to be comparable to our REFL basins. We obtained corresponding basin boundaries from the UK government's hydrology data explorer (https://environment.data.gov.uk/hydrology/explore) and DEM's from data.dov.uk. We extracted the channel networks (See Figure S1) using topotoolbox (Schwanghart and Scherler, 2014). The analysis of these British basins, including e.g. total reliefs (Table S1), channel profiles and hypsometric curves (Figure S1) show that our REFL's replicate their characteristics. Boxplots for drainage area, bankfull discharge, channel slope, bankfull width and bankfull depth are shown in Figure S3.

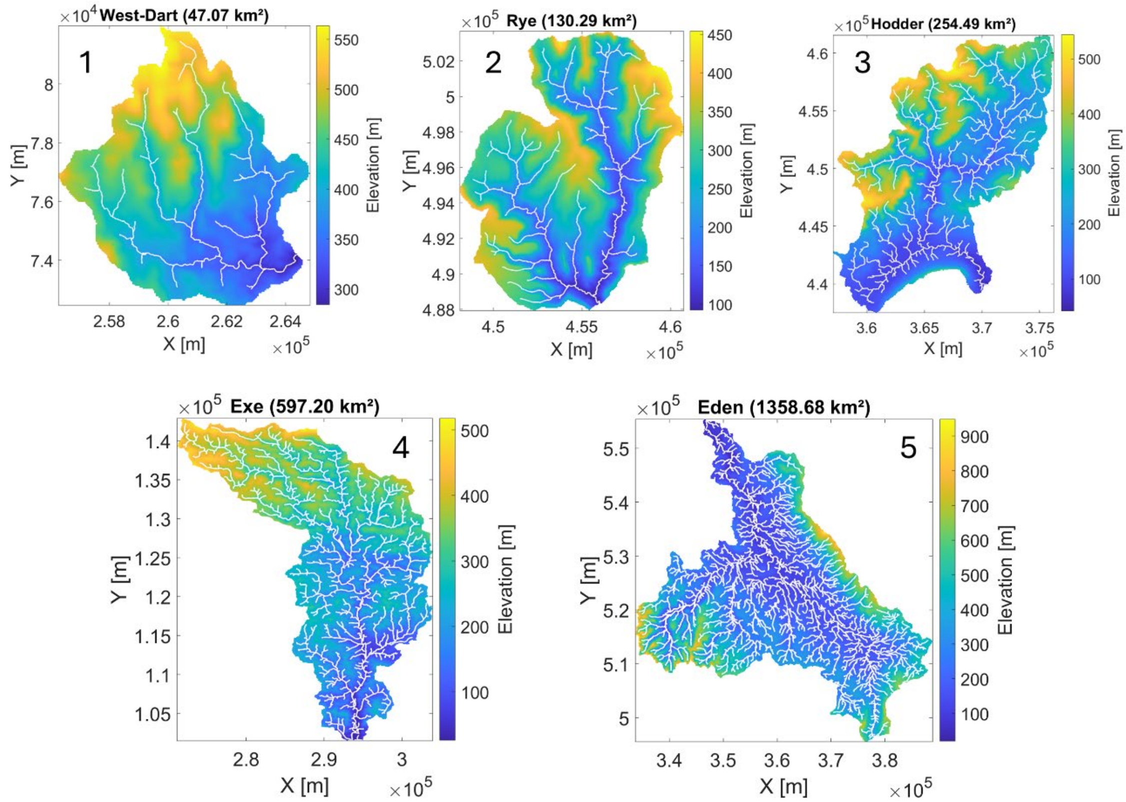

Figure S1. Channel networks extracted from DEMs of 5 different British river catchments of varying sizes chosen from the set of Hey and Thorne (see main text) given in Table S1. The channels shown here are obtained using DEM of 10m resolution and using a flow accumulation threshold of 3000 pixels.

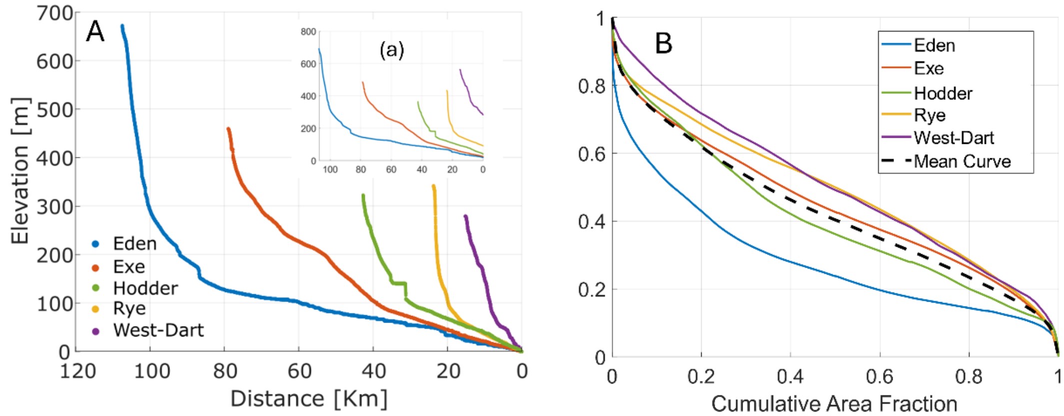

Figure S2. A) Main-stem channel profiles for the five catchments of Figure S1 with outlet elevation set to zero; (a) the same channel profiles with MSL elevations. B) Hypsometric curves for the same five catchments along with a mean hypsometric curve.

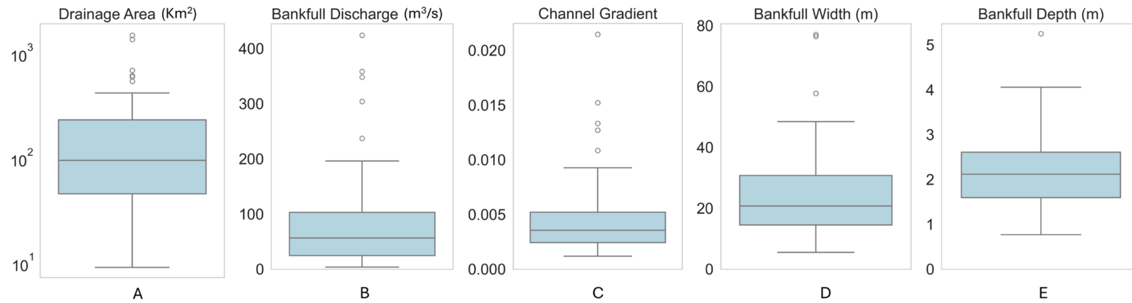

Figure S3. Range of observed properties for the 62 British streams of Table S1. Subplots A to E shows boxplots for drainage area, bankfull discharge, channel gradient (slope), bankfull width and bankfull depth respectively.

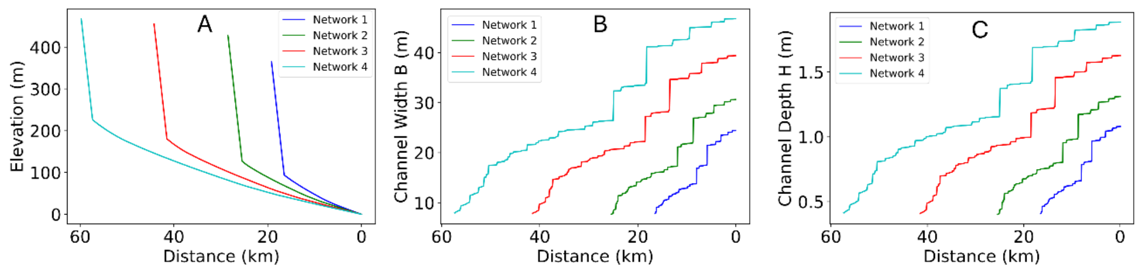

Figure S4. Characteristics of the REFL landscapes. A: elevation profiles for each landscape, from the farthest point from the outlet along the flow path corresponding to the longest channel (main stem). The constant, high slope at the upstream end of each curve corresponds to the assumed hillslope slope of 0.14. B and C: channel depth and width, respectively, for the longest channel of each landscape.

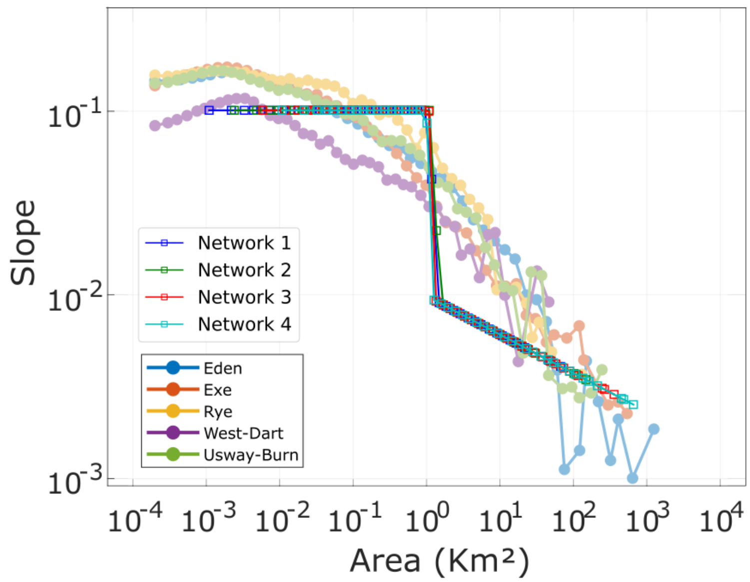

Figure S5. Slope-area relationship for the modeled REFL landscapes and the five British landscapes of Figure S1. Although the model captures the overall trend, deviation between the two sets is likely attributable to the influence of such factors as: a) downstream fining of bed material; b) mixed bedrock-alluvial channels (rather than purely alluvial) higher up in the catchment; and c) the simplified approach to hillslope length and slope in a model that does not capture the details of hillslope processes.

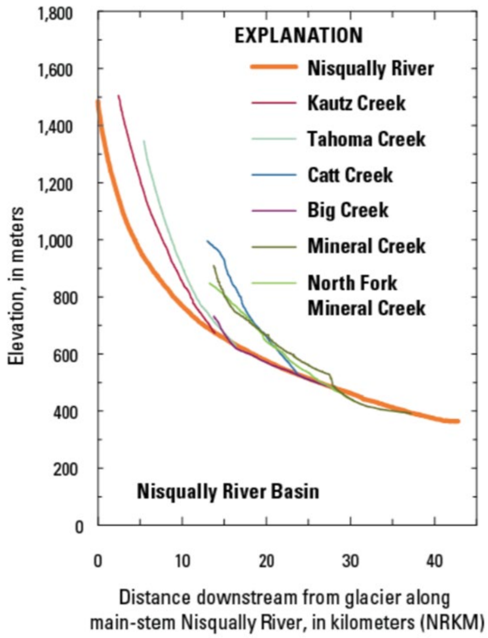

Figure S6. An example of field main-stem and tributary river profiles extracted from remotely-sensed data: Nisqually River basin, Washington, USA. (Modified from Czuba et al.; see main text). This figure bears comparison with Figures 4A and 4E pertaining to the REFL's of the present analysis.

Table S1. Characteristics of the British streams studied by Hey and Thorne (main text; values courtesy of S. Darby, University of Southampton, UK).

River	Location	Drainage Area (km^2)	Bankfull Discharge (m^3/s)	Bankfull Width (m)	Bankfull Depth (m)	Channel Gradient	Bed Material D50 (m)
Otter	Dotton	202.5	104	25.2	2.41	0.003532	0.0565
Exe	Thorverton	600.9	154	42.7	2.45	0.003159	0.0606
Exe	Stoodleigh	421.7	124	32.7	2.48	0.00255	0.0819
East Dart	Bellever	21.5	17	12.8	1.5	0.00455	0.1091
Camel	Denby	208.8	63	20	2.25	0.0042	0.0244
Fowey	Restormel	169.1	68	21.6	2.4	0.00226	0.0605
West Dart	Dunnabridge	47.9	70	27.5	2.37	0.012714	0.1758
Teign	Preston	381	148	29.4	3.29	0.0014	0.0409
Erme	Ermington	43.5	76.1	15.8	2.31	0.0064	0.0459
Neath	Resolven	190.9	172	28.7	2.94	0.00167	0.0699
Usk	Llandetty	543.9	304	48.5	3.98	0.001326	0.0657
Yscir	Pontaryscir	62.8	45	18.2	2.32	0.003	0.0668
Hirnant	Rhiwedog	33.9	50	18.4	1.82	0.01333	0.0602
Dyfrdwy	New Inn	53.9	46	20.1	1.75	0.002714	0.043
Glaslyn	Beddgelert (2)	68.6	53	25.2	1.47	0.003954	0.0747
Glaslyn	Beddgelert (1)	68.6	53	24.4	1.99	0.005119	0.0707
Alwen	Druid	184.7	69	29.7	1.54	0.003667	0.0447
Ceidog	Llandrillo	36.5	48	13	1.86	0.008202	0.0653
Lugg	Byton (1)	203.3	24	17.7	1.58	0.004	0.0481
Lugg	Byton (2)	203.3	24	21.1	1.65	0.003443	0.0348
Frome	Yarkhill	144	22	10.2	2.34	0.0022	0.0193
Pinsley Brook	Cholstrey Mill	24.2	14	10.6	1.39	0.003918	0.0139
Dove	Izaak Walton	83	7.1	13.7	0.77	0.006106	0.0483
Burbage Brook	Burbage	9.1	10	5.5	1.02	0.021467	0.1096
Manifold	Hulme End (1)	46	28	17	2.1	0.003671	0.0432
Hamps	Waterhouses	35.1	27	15	2.08	0.00482	0.0547
Churnet	Rocester	236	34	14.4	2.76	0.001339	0.0269
Rye	Broadway Foot (1)	131.7	100	25.9	3.31	0.003564	0.0808
Rye	Broadway Foot (2)	131.7	100	23	3.05	0.002775	0.0838
Snaizeholme Beck	Low Houses (1)	10.2	7.5	15.6	0.96	0.005251	0.0545
Snaizeholme Beck	Low Houses (2)	10.2	7.5	12.6	1.01	0.003429	0.086
Nidd	Birstwith	217.6	170	31.8	2.79	0.003344	0.0793
Wylye	Norton Bavant	112.4	7.1	9.6	1.2	0.001572	0.0174
Alwin	Clennel	27.7	9.7	12.3	0.97	0.010858	0.0663
Bottoms Beck	Bottoms Beck Flum	10.6	35	12.5	1.41	0.015215	0.0684
Coquet	Bygate	59.5	11.2	14.1	1.48	0.005527	0.0741
Croasedale Beck	Croasedale	10.4	53	15.2	2.06	0.009271	0.0765
Eden	Temple Sowerby	616.4	237	57.8	4.06	0.001455	0.0557
Eden	Warwick Bridge	1367	424	76.5	5.25	0.001696	0.0499
Esk	Cropple How (1)	70.2	61	22.9	1.99	0.00273	0.0534
Esk	Cropple How (2)	70.2	61	27.7	2.39	0.002636	0.0279
Glendaremeken	Threlkeld	64.5	45	18.6	2.14	0.004691	0.042
Hindurn	Wray (1)	Not Available	75	20.4	2.26	0.004256	0.0808
Hindurn	Wray (2)	Not Available	120	41.7	2.24	0.006696	0.0908
Hodder	Hodder Place	261	348	46.6	3.64	0.002961	0.066
Irthing	Greenholme	334.6	60.4	32.2	2.05	0.00119	0.0359
Kielder Burn	Kielder	58.8	36.5	28	1.9	0.005703	0.0636
Mint	Mint Bridge	65.8	74.7	19.3	2.39	0.007362	0.0584
Rede	Rede's Bridge	343.8	95	32.2	1.96	0.003816	0.1296
Sprint	Sprint Mill	34.6	50	17.5	1.81	0.00553	0.0701
Tarset Burn	Greenhaugh	96	90.5	24.6	2.91	0.003326	0.1231
Teviot	Hawick	323	126.8	31.3	2.83	0.003657	0.0711
Tweed	Boleside	1500	358.3	77.1	3.12	0.001631	0.0602
Tweed	Lyneford	373	91.3	31.2	2.22	0.001914	0.0406
Tweed	Peebles	694	153.3	33.4	2.66	0.00146	0.069
North Tyne	Tarset	284.9	192.3	45.2	3.07	0.002511	0.0916
Usway Burn	Shillmoor	21.4	17.6	9.1	1.11	0.008479	0.1135
Yarrow Water	Philiphaugh	231	196	41	2.65	0.004749	0.084
Asker	Bridport	49.1	19	11.6	2.09	0.002408	0.0183
Frome	Louds Mill	206	20	17.5	1.36	0.003557	0.0202
Chitterne Brook	Codford	Not Available	3.9	6.5	1.17	0.001935	0.0232
Manifold	Hulme End (2)	46	28	12.3	1.9	0.001891	0.0487

Table S2. Characteristics of the five British catchments shown in Figure S1. The bankfull widths and depths are the values at the outlet of each catchment.

River	**Location**	**Drainage Area (km^2)**	**Min Elevation (m)**	**Max Elevation (m)**	**Relief (m)**	**Max distance Ridge to outlet (Km)**	**Bankfull Width (m)**	**Bankfull Depth (m)**
West Dart	Dunnabridge	47	284	564	279	15	27.5	2.4
Rye	Broadway Foot (1)	130	92	454	362	24	25.9	3.3
Hodder	Hodder Place	254	42	544	503	43	46.6	3.6
Exe	Thorverton	597	26	518	492	79	42.7	2.5
Eden	Great Corby	1359	20	949	929	107	76.5	5.3
Average		478	93	606	513	54	43.8	3.4

SI Reference

Schwanghart, W., Scherler, D. (2014): TopoToolbox 2 – MATLAB-based software for topographic analysis and modeling in Earth surface sciences. Earth Surface Dynamics, 2, 1-7. [DOI: 10.5194/esurf-2-1-2014].